Rapid expansion of oceanic anoxia immediately before the end-Permian mass extinction

Gregory A. Brennecka[a,1], Achim D. Herrmann[a,b], Thomas J. Algeo[c], and Ariel D. Anbar[a,d]

[a]School of Earth and Space Exploration, Arizona State University, P.O. Box 871404, Tempe, AZ 85287-1404; [b]Barrett, the Honors College, Arizona State University, Tempe, AZ 85287-1612; [c]Department of Geology, University of Cincinnati, Cincinnati, OH 45221-0013; and [d]Department of Chemistry and Biochemistry, Arizona State University, Tempe, AZ 85287-1404

Edited by Donald E. Canfield, University of Southern Denmark, Odense M., Denmark, and approved September 11, 2011 (received for review April 18, 2011)

Periods of oceanic anoxia have had a major influence on the evolutionary history of Earth and are often contemporaneous with mass extinction events. Changes in global (as opposed to local) redox conditions can be potentially evaluated using U system proxies. The intensity and timing of oceanic redox changes associated with the end-Permian extinction horizon (EH) were assessed from variations in $^{238}U/^{235}U$ ($\delta^{238}U$) and Th/U ratios in a carbonate section at Dawen in southern China. The EH is characterized by shifts toward lower $\delta^{238}U$ values (from −0.37‰ to −0.65‰), indicative of an expansion of oceanic anoxia, and higher Th/U ratios (from 0.06 to 0.42), indicative of drawdown of U concentrations in seawater. Using a mass balance model, we estimate that this isotopic shift represents a sixfold increase in the flux of U to anoxic facies, implying a corresponding increase in the extent of oceanic anoxia. The intensification of oceanic anoxia coincided with, or slightly preceded, the EH and persisted for an interval of at least 40,000 to 50,000 y following the EH. These findings challenge previous hypotheses of an extended period of whole-ocean anoxia prior to the end-Permian extinction.

carbonates | uranium isotopes | paleoredox

The end-Permian extinction represents the largest mass extinction in Earth history, with the demise of an estimated 90% of all marine species (1). While it has been extensively studied, the exact nature and cause of the end-Permian extinction remains the subject of intense scientific debate. Proposed kill mechanisms have included a nearby supernova, bolide impacts, periods of extreme volcanism (e.g., Siberian Traps), extensive glaciation, and widespread oceanic anoxia (2). Evidence for shallow-ocean anoxia in conjunction with the end-Permian mass extinction is widespread (3–6), but the intensity and timing of oceanic redox changes remain uncertain (7–10). Recent hypotheses have invoked the release of hydrogen sulfide gas (H_2S) from seawater as a kill mechanism (11–13). Such models call upon strong expansion of oceanic anoxia below the oxygenated surface layer to allow buildup of H_2S, followed by an upward excursion of the chemocline that releases the poisonous gas into the atmosphere (13). In this study, we examine the $^{238}U/^{235}U$ and Th/U (thorium/uranium) ratios in a carbonate section spanning the end-Permian extinction horizon (EH) to evaluate the timing and scale of these possibilities. Samples for this study were collected from the Dawen section of the Yangtze Block in southern China (Fig. 1), which has been correlated with the global stratotype section and point (GSSP) of the Permian-Triassic boundary at Meishan (14).

Due to the geochemical properties of U, the ratio of $^{238}U/^{235}U$ can be used as a tool to investigate the history of ocean oxygenation at a global scale, as opposed to the local redox information provided by most commonly used proxies. The long residence time (~500 ky) of U in the oceans leads to a homogeneous U concentration in seawater (15, 16), as well as to a homogenous U isotopic composition (17–19). The low-temperature redox transition of U (from U^{6+} to U^{4+}) is the primary cause of $^{238}U/^{235}U$ fractionation on Earth, with the reduced species preferentially enriched in ^{238}U (18–22). During times of oceanic anoxia, the flux of reduced U to anoxic facies (such as black shales) increases, preferentially removing ^{238}U from seawater. The loss of isotopically heavy U drives seawater to lighter isotopic compositions (23). Changes in the U isotope ratios of organic-rich sediments have been used to study oceanic redox conditions during the Cretaceous (23). Here, we apply this isotope system to Late Permian and Early Triassic carbonate rocks. Existing evidence indicates that carbonates record the $^{238}U/^{235}U$ ratio of the seawater in which they were deposited (18, 19), suggesting that ancient carbonates that retain a primary signal of U isotopes can be used to estimate relative changes in ocean oxygenation.

Results and Discussion

In the Dawen section, the average U isotopic composition of samples deposited prior to the EH ($\delta^{238}U = -0.37‰$) is very close to that of modern seawater [$\delta^{238}U = -0.41 \pm 0.03‰$ (19)]. This observation suggests that the fraction of U removed to reducing sinks during the late Permian was similar to that of the modern ocean. The Dawen section exhibits an abrupt and significant change in $\delta^{238}U$ at the EH (Fig. 2) to values averaging −0.65‰. The $\delta^{238}U$ ratios of pre- and post-EH samples are significantly different ($p < 0.0001$; two-tailed student's t-test with a significance level of $\alpha = 0.01$). A few isotopically light samples are present below the EH (−118 and −97 cm), which may provide evidence of brief episodes of transient intensification of oceanic anoxia preceding the end-Permian mass extinction. This inference is supported by evidence from additional geochemical proxies in other studies (7) (see *SI Text* for further discussion).

The shift toward lighter U isotopic compositions after the extinction event is consistent with an increase in the deposition of isotopically heavy U in anoxic facies. The isotopic composition of U in seawater is ultimately controlled by the relative sizes and isotopic signatures of the major sources and sinks of U to the ocean. A simple box model of the oceanic U budget for the modern and end-Permian oceans is shown in Fig. 3. Invoking mass balance, we calculated the approximate increase in anoxic sedimentation in the end-Permian ocean as:

$$\delta^{238}U_{input} = ((1 - f_{anoxic}) \times \delta^{238}U_{other}) + (f_{anoxic} \times \delta^{238}U_{anoxic}). \quad [1]$$

Here, f_{anoxic} represents the fraction of U deposited in anoxic facies and $\delta^{238}U$ represents the $\delta^{238}U$ values of the anoxic and "other" (i.e., nonanoxic) sinks. Following Montoya-Pino, et al. (23), we assume: (1) isotopically constant U input from rivers [the largest source of U to the ocean (24)] over geologic time with

Author contributions: G.A.B., A.D.H., and A.D.A. designed research; G.A.B. and T.J.A. performed research; G.A.B., A.D.H., and T.J.A. analyzed data; and G.A.B., A.D.H., T.J.A., and A.D.A. wrote the paper.

The authors declare no conflict of interest.

This article is a PNAS Direct Submission.

[1]To whom correspondence should be addressed. E-mail: brennecka@asu.edu.

This article contains supporting information online at www.pnas.org/lookup/suppl/doi:10.1073/pnas.1106039108/-/DCSupplemental.

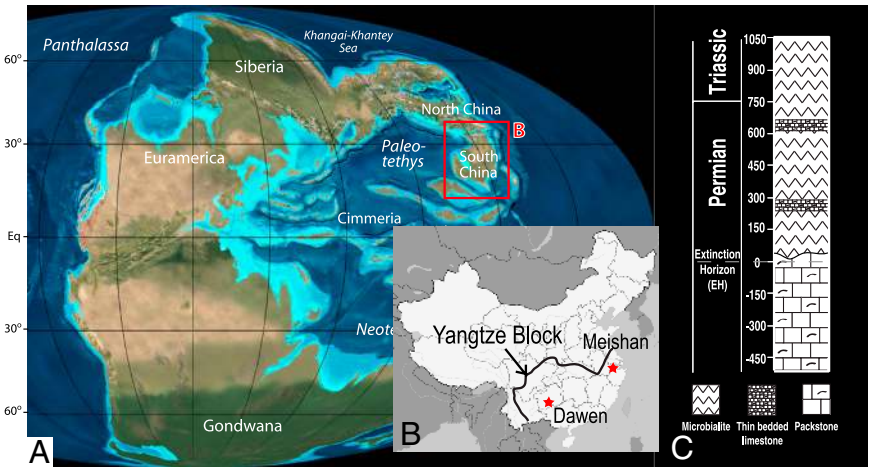

Fig. 1. Location of South China at ~252 Ma, the time of the end-Permian extinction [Fig. 1*A*, modified base map from R. Blakey (http://jan.ucc.nau.edu/~rcb7/260moll.jpg)] and present-day location of the Dawen section (Fig. 1*B*, modified from ref. 14). The location of the Meishan GSSP is shown for reference. Lithostratigraphy of the Dawen section is shown in Fig. 1*C*; see ref. 14 for its correlation to the Meishan GSSP.

a value of −0.3‰; (2) a constant isotope fractionation between seawater and anoxic/euxinic environments of +0.5‰; and (3) a constant (+0.1‰) isotope fractionation between seawater and the sum of other sinks, including ferromanganese oxide, hydrothermal, and suboxic sediments. Suboxic sediments, which are defined by their low oxygen concentrations in the bottom water [e.g., 0.2–2 mL O_2 per1 H_2O (25)], are likely to represent the largest nonanoxic sink (24) and are known to accumulate U with a small fractionation (+0.1‰) relative to seawater (19). Based on the assumptions above, $\delta^{238}U_{input} = -0.3‰$, $\delta^{238}U_{other} = -0.55‰$ (i.e., $-0.65 + 0.1‰$), and $\delta^{238}U_{anoxic} = -0.15‰$ (i.e., $-0.65 + 0.5‰$). These values yield an estimated sixfold increase in the flux of U to anoxic facies in conjunction with the EH.

Th/U ratios serve as an additional and independent line of evidence for oceanic redox changes in conjunction with the end-Permian extinction. Previous workers have used Th/U ratios in reduced sediments as a proxy for ocean redox chemistry (5). As Th has only one redox state (Th^{4+}), its concentration in sediments is unaffected by redox conditions. On the other hand, U is a redox-sensitive metal and is readily removed from seawater as insoluble U^{4+} under reducing conditions (26–28), thus concentrating U relative to Th in anoxic facies. An increase in anoxic sedimentation reduces the concentration of U in seawater as more U is sequestered in organic-rich sediments. Because the U concentration of carbonates is related to the U concentration of the seawater in which they are deposited (29, 30), an increase in anoxic sedimentation results in an increase in the Th/U ratio of carbonate sediments. At Dawen, average Th/U ratios increase from 0.06 below the EH to 0.42 above the EH (Fig. 2). This increase reflects a decrease in the U content of seawater, possibly by a factor of ~7× if Th concentrations remained constant. A change in seawater U concentrations of this magnitude is consistent with the sixfold expansion of oceanic anoxic inferred from our $\delta^{238}U$ data, and is also consistent with the sharp decrease in U concentrations across the Permian-Triassic boundary (PTB) previously reported from a carbonate section in Oman (10). Although a lower U concentration would imply a shorter ocean residence time, even if reduced tenfold the U residence time would have been 50–100 times longer than the time scale for ocean mixing. Therefore, it is reasonable to assume that $\delta^{238}U$ and Th/U provide information at global scale.

Although the study section has undergone burial diagenesis, the U and carbonate C isotopic profiles are unlikely to have been

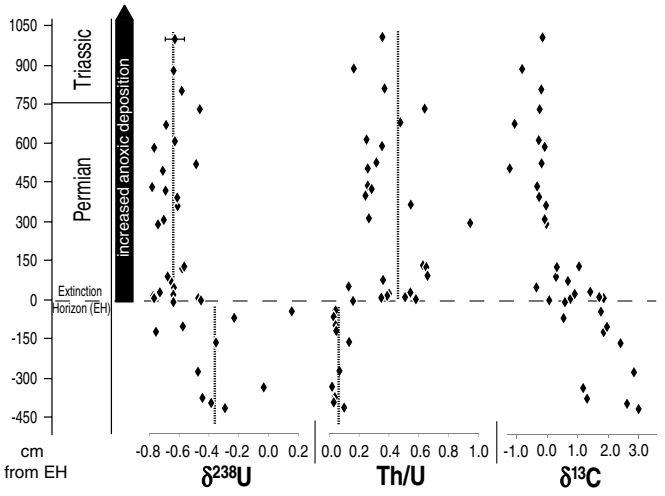

Fig. 2. Geochemical profiles for the Dawen section. The vertical dashed lines represent average values of $\delta^{238}U$ and Th/U for pre-EH and post-EH samples. The $^{238}U/^{235}U$ ratios are reported using standard δ-notation, where $\delta^{238}U = [Ratio_{meas}/Ratio_{std(SRM950a)} - 1] \times 1{,}000$. Average 2 × standard deviation (2SD) uncertainty of $\delta^{238}U$ values is shown on the top data point only for clarity. $\delta^{13}C$ and stratigraphic data from ref. 14.

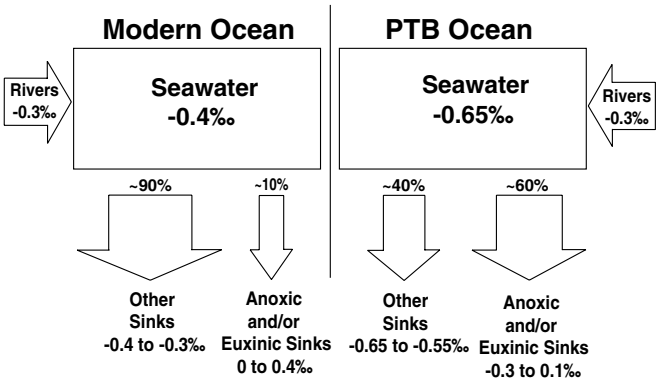

Fig. 3. Box models representing the modern ocean (left) and the hypothesized end-Permian anoxic ocean on the right. Estimates of the percentage of U flux for each sink are shown above the arrows. All data are displayed using standard δ-notation, as defined above. Modern $\delta^{238}U$ values are taken from Weyer, et al. (19). The values from the PTB ocean (right) are based on calculations using the average $\delta^{238}U$ of carbonates after the EH in our sample set (see Eq. **1**) and assuming a constant isotope fractionation between seawater and anoxic sediments.

altered greatly. For example, neither $\delta^{238}U$ nor Th/U shows a correlation with degree of dolomitization or with terrigenous input; see *SI Text* for discussion.

The timing for the onset of widespread oceanic anoxia implied by our results from Dawen is difficult to reconcile with previous hypotheses of persistent anoxia for hundreds of thousands or millions of years prior to the end-Permian extinction event (3, 5, 6, 8). The abrupt increase in Th/U ratios and decrease in $\delta^{238}U$ that begin at or just below the EH indicate that sustained expanded anoxia did not exist in the Late Permian ocean until immediately prior to the extinction event. This global redox signal is consistent with proxies recording local redox conditions within the Panthalassic Ocean (31, 32). In contrast, the steady and prolonged decline of carbonate $\delta^{13}C$ seen in many stratigraphic sections prior to the EH has been used to argue for an extended period of ocean stagnation and whole-ocean anoxia (2). If so, $\delta^{238}U$ and Th/U in carbonates should track $\delta^{13}C$. This behavior is not observed (Fig. 2).

The existence of an unconformable surface in the Dawen section at the level of the EH (Fig. 2) makes exact assessment of the timing of global redox changes unattainable. If the missing section is equivalent to beds 25 and 26 at Meishan, it would represent a hiatus of about 50,000–75,000 y (14). However, we note that the $\delta^{13}C$ curve for Dawen (see Fig. 5 in ref. 14) shows an almost unbroken shift toward more negative values across the contact, suggesting that the hiatus was of limited duration. These data indicate that the abruptness of the shifts in $\delta^{238}U$ and Th/U ratios at the EH (Fig. 2) was the result not of a missing section but, rather, of a rapid and sustained change in oceanographic conditions. The persistence of low $\delta^{238}U$ and high Th/U ratios through the 10 m of section above the EH that were analyzed in this study (Fig. 2) indicates that intensified anoxia persisted a minimum of ~40,000–50,000 y following the end-Permian extinction (14, 33, 34).*

While our data do not support the extended period of whole-ocean anoxia prior to the EH inferred from $\delta^{13}C$ records, they do not invalidate the idea that the end-Permian mass extinction was caused by oceanic oxygen depletion and a subsequent build-up and release of H_2S from the oceans, as inferred on the basis of geochemical, isotopic, and biomarker studies (3–6, 8). Commonly, models of this process invoke an extended period of sluggish ocean circulation, producing deep-ocean anoxia and accumulation of H_2S. This interpretation was previously challenged by numerical models of the ocean-climate system suggesting that the deep ocean was most likely well ventilated throughout the Late Permian-Early Triassic interval (35). We propose that the geochemical data and numerical models can be reconciled by hypothesizing expanded and more intense oxygen-minimum zones at middepths in the late-Permian ocean (7, 9, 32). Suboxic deep-ocean conditions during the Late Permian prior to the EH (9, 32) would have decreased the U concentration of the ocean, lowering the residence time of U in seawater and setting the stage for the rapid shift in Th/U at the EH observed at Dawen (Fig. 2). Th/U ratios of pre-EH carbonates at Dawen are significantly higher than Th/U ratios in modern marine carbonates, supporting the hypothesis that U was substantially drawn down in latest Permian seawater relative to modern seawater. Suboxic deep-ocean conditions would not have markedly altered the U isotope budget of the global ocean, as suboxic sedimentation does not fractionate U isotopes with the same magnitude as anoxic sedimentation (19, 23). Uranium isotopes would have shifted measurably only with an increase in anoxic sedimentation. However, transient disturbances to Late Permian oceans [e.g., warming or an increase in continentally derived nutrients (9)] may have resulted in brief episodes of expansion of oxygen-minimum zones before the end-Permian extinction, as reflected in light $\delta^{238}U$ ratios below the EH (−118 and −97 cm). Expansion of oxygen-minimum zones could have introduced H_2S into the photic zone (9) if the upper boundary of the former shallowed sufficiently (to <100 m water depth). This could then result in release of toxic gasses into shallow-marine environments and the atmosphere (12), similar to the degassing of H_2S in modern oxygen-minimum zones in Namibia (36).

A model of ocean chemistry with widespread regions of relatively warm and poorly oxygenated deep water and localized intermittent sulfide maxima at midwater depths (i.e., within the oxygen-minimum zone) satisfies not only $\delta^{13}C$ evidence previously used to argue for sustained oceanic anoxia prior to the EH, but also explains the observed geochemical and biogeochemical signatures associated with anoxia/euxinia at the close of the Permian. Development of middepth sulfide maxima poised on the edge of expansion into the surface water layer could account for the presence of biomarkers indicative of photic-zone euxinia in shallow-marine sections prior to the EH (4, 6) without requiring anoxia of the deep ocean, which would alter the U isotope budget of seawater. Evidence from the U system indicates widespread oceanic anoxia only became pronounced and persistent at, or just preceding the EH. Thus, this study supports the possibility of H_2S as a killing mechanism, but calls for buildup of H_2S in the oxygen-minimum zone rather than prolonged accumulation in the deep ocean. This interpretation should be tested by investigating U proxies across other Permian-Triassic sections and by examining the fidelity with which carbonate sediments record and preserve primary U proxy signatures.

Methods

Study samples were powdered and dissolved using dilute (~1 M) hydrochloric acid, leaving any noncarbonate species present (e.g., organics, pyrite, siliciclastics, etc .....) intact and nonparticipatory in subsequent procedures. The dissolved material was dried and reconstituted in 3 M HNO_3. Approximately 10% of the material was used for trace element analyses, with data obtained using a Thermo X-series quadrupole ICP-MS at the W. M. Keck Laboratory for Environmental Biogeochemistry at Arizona State University (ASU). The remaining 90% of the dissolved carbonate material was passed through a column containing Eichrom® UTEVA resin, following the procedure outlined in Weyer, et al. (19) to separate uranium from the matrix. Uranium isotope measurements were performed on a ThermoFinnigan Neptune MC-ICP-MS instrument at Arizona State University (ASU, W.M. Keck Laboratory for Environmental Biogeochemistry), utilizing a ^{236}U:^{233}U double-spike MC-ICP-MS procedure described in Weyer, et al. (19). The isotopic composition of the double spike used is $^{236}U/^{233}U = 1.00494$, $^{238}U/^{233}U = 0.000958$, $^{235}U/^{233}U = 0.000108$. Samples were spiked to achieve ^{236}U and ^{233}U signals of ~2.5 times the voltage on the least abundant measured isotope, ^{235}U. This spiking technique maximizes the counting statistics on the spike masses, while minimizing the tailing contributions at mass 235. All measured isotopes of U were collected by a Faraday cup collector array, utilizing 10^{11} ohm resistors for all masses. Samples dissolved in 2% HNO_3 were introduced with an Apex-Q sample introduction system. Optimum precision was obtained running samples at ~100 ppb U. The U isotope standards SRM950a and CRM129a were measured bracketing samples as checks for run reproducibility and consistency. External reproducibility based on multiple runs of the SRM950a and CRM129a standards over the course of this study is shown in *SI Text*. The U isotopic compositions of the samples are reported as relative to the U isotope standard SRM950a.

ACKNOWLEDGMENTS. We thank the W.M. Keck Laboratory for Environmental Biogeochemistry and G. Gordon for technical assistance with U, Th, and $\delta^{238}U$ analyses. We are grateful to L. Borg and R. Williams for assistance with the U double spike and to S. Romaniello for many helpful discussions. We also thank two anonymous reviewers for helpful comments that greatly improved the manuscript. This work was supported by the NASA Astrobiology Institute, the NASA Exobiology Program, and by National Science Foundation (NSF) grant OCE-0952394.

*The duration of the Griesbachian is constrained by refs. 33, 34. The ~730-ky-long Griesbachian at Dawen is ~160 m thick, therefore the first 10 m represents ~40,000–50,000 y, assuming constant sedimentation rates. A similar result is achieved by using data from ref. 14, which estimates that the stratigraphic equivalent of Beds 25 through 28 at Meishan is the lower ~30 m at Dawen. The duration of this interval was estimated at 150,000 y, therefore the lower 10 m at Dawen represent ~50,000 y.

1. Stanley SM (2007) An analysis of the history of marine animal diversity. *Paleobiology* 33:1–55.
2. Erwin DH, Bowring SA, Yugan J (2002) *Catastrophic Events and Mass Extinctions: Impacts and Beyond: Geological Society of America Special Paper*, eds C Koeberl and KG MacLeod pp 363–383.
3. Bond DPG, Wignall PB (2010) Pyrite framboid study of marine Permian-Triassic boundary sections: a complex anoxic event and its relationship to contemporaneous mass extinction. *Geol Soc Am Bull* 122:1265–1279.
4. Grice K, et al. (2005) Photic zone euxinia during the Permian-Triassic superanoxic event. *Science* 307:706–709.
5. Wignall PB, Twitchett RJ (1996) Ocean anoxia and the end-Permian mass extinction. *Science* 272:1155–1158.
6. Cao C, et al. (2009) Biogeochemical evidence for euxinic oceans and ecological disturbance presaging the end-Permian mass extinction event. *Earth Planet SC Lett* 281:188–201.
7. Algeo TJ, et al. (2010) Changes in productivity and redox conditions in the Panthalassic Ocean during the latest Permian. *Geology* 38:187–190.
8. Isozaki Y (1997) Permian-Triassic boundary superanoxia and stratified superocean: records from lost deep sea. *Science* 276:235–238.
9. Algeo TJ, Chen ZQ, Fraiser ML, Twitchett RJ (2011) Terrestrial-marine teleconnections in the collapse and rebuilding of Early Triassic marine ecosystems. *Palaeogeography Palaeoclimatology Palaeoecology* 308:1–11.
10. Ehrenberg SN, Svånå TA, Swart PK (2008) Uranium depletion across the Permian-Triassic boundary in Middle East carbonates: Signature of oceanic anoxia. *AAPG Bull* 92:691–707.
11. Kump LR, Pavlov A, Arthur MA (2005) Massive release of hydrogen sulfide to the surface ocean and atmosphere during intervals of oceanic anoxia. *Geology* 33:397–400.
12. Meyer KM, Kump LR, Ridgwell A (2008) The biogeochemical controls on photic-zone euxinia during the end-Permian mass extinction. *Geology* 36:747–750.
13. Riccardi A, Kump LR, Arthur MA, D'Hondt S (2007) Carbon isotopic evidence for chemocline upward excursions during the end-Permian event. *Palaeogeography, Palaeoclimatology, Palaeoecology* 248:73–81.
14. Chen J, Beatty TW, Henderson CM, Rowe H (2009) Conodont biostratigraphy across the Permian-Triassic boundary at the Dawen section, Great Bank of Guizhou, Guizhou Province, South China: implications for the Late Permian extinction and correlation with Meishan. *J Asian Earth Sci* 36:442–458.
15. Klinkhammer GP, Palmer MR (1991) Uranium in the oceans: where it goes and why. *Geochimica et Cosmochimica Acta* 55:1799–1806.
16. Ku T.-L, Knauss K, Mathieu GG (1977) Uranium in the open ocean: concentration and isotopic composition. *Deep-sea res* 24:1005–1017.
17. Delanghe D, Bard E, Hamelin B (2002) New TIMS constraints on the uranium-238 and uranium-234 in seawaters from the main ocean basins and the Mediterranean Sea. *Mar Chem* 80:79–93.
18. Stirling CH, Anderson MB, Potter E.-K, Halliday A (2007) Low-temperature isotopic fractionation of uranium. *Earth Planet SC Lett* 264:208–225.
19. Weyer S, et al. (2008) Natural fractionation of $^{238}U/^{235}U$. *Geochimica et Cosmochimica Acta* 72:345–359.
20. Bopp CJ, Lundstrom CC, Johnson TM, Glessner JJG (2009) Variations in $^{238}U/^{235}U$ in uranium ore deposits: isotopic signatures of the U reduction process? *Geology* 37:611–614.
21. Brennecka GA, Borg LE, Hutcheon ID, Sharp MA, Anbar AD (2010) Natural variations in uranium isotope ratios of uranium ore concentrates: understanding the $^{238}U/^{235}U$ fractionation mechanism. *Earth Planet SC Lett* 291:228–233.
22. Bopp CJ, et al. (2010) Uranium $^{238}U/^{235}U$ isotope ratios as indicators of reduction: results from an in situ biostimulation experiment at Rifle, Colorado, USA. *Environmental Science and Technology* 44:5927–5933.
23. Montoya-Pino C, et al. (2010) Global enhancement of ocean anoxia during Oceanic Anoxic Event 2: a quantitative approach using U isotopes. *Geology* 38:315–318.
24. Dunk RM, Mills RA, Jenkins WJ (2002) A reevaluation of the oceanic uranium budget for the Holocene. *Chem Geol* 190:45–67.
25. Tyson RV, Pearson TH (1991) Modern and ancient continental shelf anoxia: an overview. *Modern and Ancient Continental Shelf Anoxia*, eds RV Tyson and TH Pearson (Geololgical Society Special Publications, London), vol. 58, pp 1–26.
26. Anderson RF, Fleisher MQ, Lehuray AP (1989) Concentration, oxidation-state, and particulate flux of uranium in the Black-Sea. *Geochimica et Cosmochimica Acta* 53:2215–2224.
27. McManus J, et al. (2006) Molybdenum and uranium geochemistry in continental margin sediments: paleoproxy potential. *Geochimica et Cosmochimica Acta* 70:4643–4662.
28. Morford JL, Emerson S (1999) The geochemistry of redox sensitive trace metals in sediments. *Geochimica et Cosmochimica Acta* 63:1735–1750.
29. Gvirtzman G, Friedman GM, Miller DS (1973) Control and distribution of uranium in coral reefs during diagenesis. *J Sediment Res* 43:985–997.
30. Shen GT, Dunbar RB (1995) Environmental controls on uranium in reef corals. *Geochimica et Cosmochimica Acta* 59:2009–2024.
31. Wignall PB, et al. (2010) An 80 million year oceanic redox history from Permian to Jurassic pelagic sediments of the Mino-Tamba terrane, SW Japan, and the origin of four mass extinctions. *Global and Planet Change* 71:109–123.
32. Algeo TJ, et al. (2011) Spatial variation in sediment fluxes, redox conditions, and productivity in the Permian-Triassic Panthalassic Ocean. *Palaeogeography, Palaeoclimatology, Palaeoecology* 308:65–83.
33. Mundil R, Palfry J, Renne PR, Brack P (2010) *The Triassic Timescale Geological Society*, ed SG Lucas (Special Publications, London), 41–60.
34. Guo G, Tong J, Zhang S, Zhang J, Bai L (2008) Cyclostratigraphy of the Induan (Early Triassic) in West Pingdingshan Section, Chaohu, Anhui Province. *Sci China Ser D* 51:22–29.
35. Winguth AME, Maier-Reimer E (2005) Causes of the marine productivity and oxygen changes associated with the Permian-Triassic boundary: a reevaluation with ocean general circulation models. *Mar Geol* 217:283–304.
36. Brüchert V, Currie B, Peard KR (2009) Hydrogen sulphide and methane emissions on the central Namibian shelf. *Prog Oceanogr* 83:169–179.

Supporting Information

Brennecka et al. 10.1073/pnas.1106039108

SI Text

Reproducibility of Uranium (U) Isotope Data. External reproducibility based on multiple runs of the U isotope standards SRM950a and CRM129a over the course of this study is shown in Fig. S1. The U isotopic compositions of the samples are reported as relative to the U isotope standard SRM950a. Sample data from all runs are shown in Table S1.

Discussion on Secondary Alteration. Due to the reactivity of carbonate sediments, diagenetic alteration of samples is a potential concern. Fluctuations of δ^{238}U values in samples immediately below the extinction horizon (EH) at Dawen may indicate instability in the redox state of the ocean preceding the end-Permian extinction (1); however because these fluctuations are not seen in the thorium/uranium (Th/U) ratios of the same samples, they could be the result of secondary processes such as addition of isotopically heavy U. Given our current understanding of the U isotope system, no secondary process is known to generate isotopically lighter δ^{238}U values in carbonates, although secondary redox precipitation of U would produce heavy δ^{238}U in diagenetically altered samples (2–4).

Although it is difficult to rule out diagenesis in carbonate samples, several considerations support our interpretation that variation in both δ^{238}U and Th/U at Dawen is mainly of primary origin. First, the major changes in both Th/U and δ^{238}U occur at, or immediately preceding, the EH. Data from δ^{238}U and Th/U are independent of one another, and both fit previously proposed models for isotopic and elemental response to ocean anoxia from other basins (5). The fact that the Dawen section displays a similar trend of U chemistry across the Permian-Triassic boundary as in Oman (5) argues for a global cause, rather than local diagenetic processes. Secondly, our current understanding of U chemistry in marine sediments argues against the local effects of diagenesis. The possibilities of altering the δ^{238}U and Th/U of the samples are primarily limited to (*i*) secondary precipitation of U, and (*ii*) removal of U from the system. In the first case, precipitation of U-containing calcium carbonate cement as a secondary process is generally an early diagenetic process (6) and would thus reflect seawater values as well. Precipitation of uranium-bearing carbonate containing cements during late stage burial diagenesis could shift the isotopic values of the carbonate sediments; however, the conclusions that we are drawing would still be valid, even when assuming that the entire section has undergone some late burial cement precipitation, as the temporal trends should not change in a relative sense. In the second case, if U was leached from the Dawen samples during burial, only the Th/U ratio would be affected with δ^{238}U remaining unchanged. Unlike ^{234}U, which is concentrated in the aqueous phase by preferential leaching of alpha-recoil damage sites from the decay of ^{238}U (7), leaching of U has been shown not to measurably alter the ^{238}U/^{235}U ratio of sediments (3, 4, 8). Furthermore, it has been suggested that because U is incorporated into the calcium carbonate as a uranyl complex as part of a dilute solid solution, remobilization of U would require bulk dissolution (9, 10). This process should have no effect on the isotopic composition of the residual carbonate material as no leaching has taken place.

The carbonate δ^{13}C curve for Dawen shows good correspondence to δ^{13}C curves at other Permian-Triassic boundary sections, so it is unlikely that bulk carbonate δ^{13}C has been modified to any significant degree by diagenesis. Further, the carbonate sediment at Dawen appears to have stabilized early in the burial environment, as reflected in relatively heavy δ^{18}O values, which average $-4.6 \pm 1.7‰$ ($n = 75$). The absence of negative δ^{18}O outliers is also an indication of little, if any, late-stage diagenesis. These considerations are consistent with the idea that the carbonate δ^{13}C curve is a record of primary marine δ^{13}C values, adding confidence that U isotopes and Th/U signals are primary in origin.

The concentration of aluminum (Al) was obtained on the samples as an indicator of terrigenous input and is shown as U/Al. No correlation exists between U/Al and δ^{238}U or Th/U in these samples (Fig. S2), so it is unlikely that the large changes in δ^{238}U and Th/U across the EH were caused by terrigenous input of U. Similarly, lithology is unlikely to have controlled the δ^{238}U and Th/U of samples, as the degree of dolomitization shows no correlation with δ^{238}U and only a weak correlation with Th/U ratio ($R^2 = 0.24$).

1. Algeo TJ, et al. (2010) Changes in productivity and redox conditions in the Panthalassic Ocean during the latest Permian. *Geology* 38:187–190.
2. Weyer S, et al. (2008) Natural fractionation of ^{238}U/^{235}U. *Geochimica et Cosmochimica Acta* 72:345–359.
3. Bopp CJ, Lundstrom CC, Johnson TM, Glessner JJG (2009) Variations in ^{238}U/^{235}U in uranium ore deposits: isotopic signatures of the U reduction process? *Geology* 37:611–614.
4. Brennecka GA, Borg LE, Hutcheon ID, Sharp MA, Anbar AD (2010) Natural variations in uranium isotope ratios of uranium ore concentrates: understanding the ^{238}U/^{235}U fractionation mechanism. *Earth and Planetary Science Letters* 291:228–233.
5. Gvirtzman G, Friedman GM, Miller DS (1973) Control and distribution of uranium in coral reefs during diagenesis. *Journal of Sedimentary Research* 43:985–997.
6. Ehrenberg SN, Svånå TA, Swart PK (2008) Uranium depletion across the Permian–Triassic boundary in Middle East carbonates: signature of oceanic anoxia. *AAPG Bulletin* 92:691–707.
7. Kigoshi K (1971) Alpha-recoil thorium-234: dissolution into water and uranium-234/uranium-238 disequilibrium in nature. *Science* 173:47–48.
8. Stirling CH, Anderson MB, Potter EK, Halliday A (2007) Low-temperature isotopic fractionation of uranium. *Earth and Planetary Science Letters* 264:208–225.
9. Reeder RJ, Nugent M, Lamble GM, Tait CD, Morris DE (2000) Uranyl incorporation into calcite and aragonite: XAFS and luminescence studies. *Environmental Science and Technology* 34:638–644.
10. Swart PK, Hubbard J (1982) Uranium in scleractinian coral skeletons. *Coral Reefs* 1:13–19.
11. Chen, J, Beatty TW, Henderson CM, Rowe H (2009) Conodont biostratigraphy across the Permian-Triassic boundary at the Dawen section, Great Bank of Guizhou, Guizhou Province, South China: implications for the Late Permian extinction and correlation with Meishan. *Journal of Asian Earth Sciences* 36:442–458.

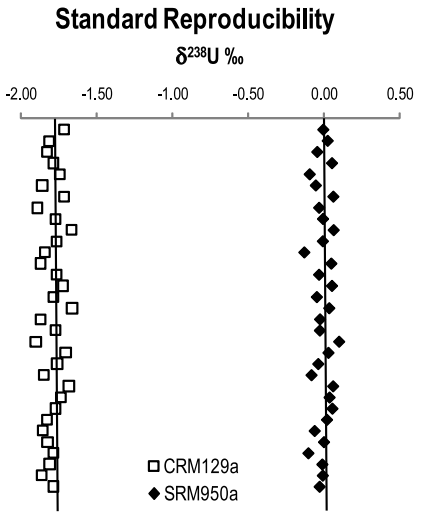

Fig. S1. The long-term external reproducibilities of the SRM950a and CRM129a standards for analyses performed during this study, relative to SRM950a. The solid vertical lines represent the average of all analyses for each standard; average values are 0.00 ± 0.11 and -1.79 ± 0.13 for SRM950a and CRM129a, respectively, with uncertainties given as $2 \times$ standard deviation (2SD).

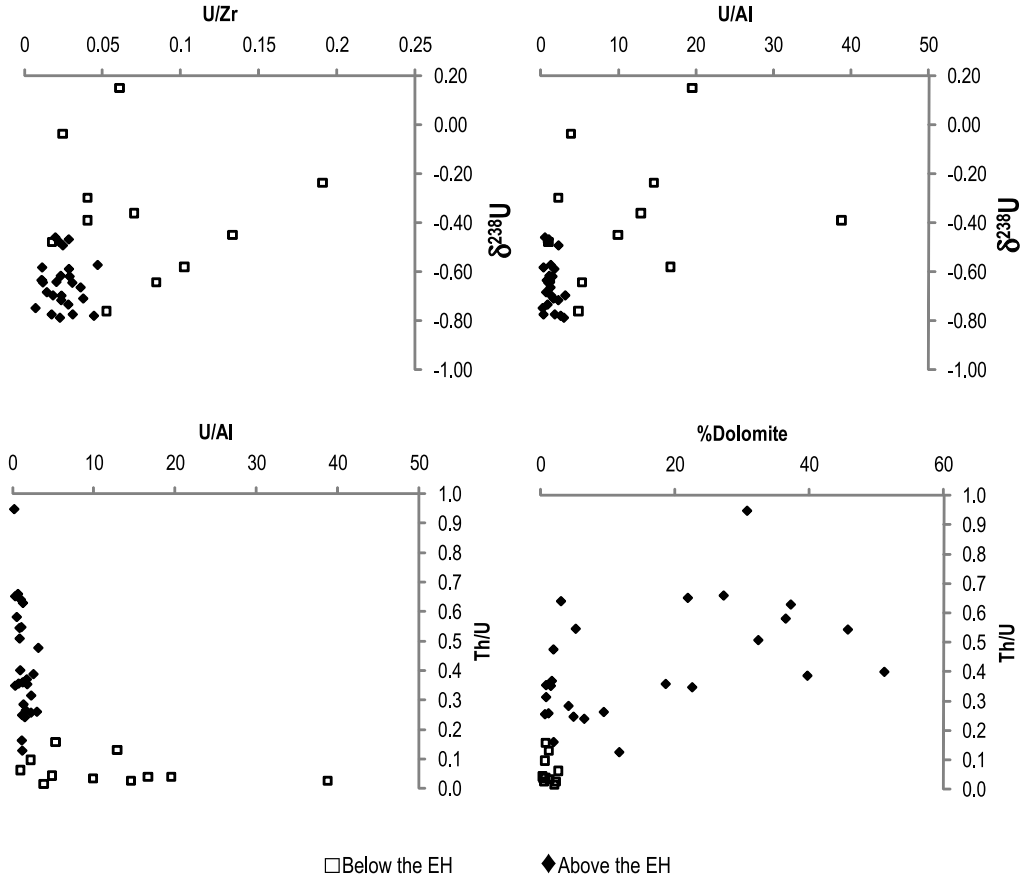

Fig. S2. Crossplots of U/Al and %Dolomite vs. Th/U and δ^{238}U. Open squares represent samples below the EH, closed diamonds represent samples above the EH.

Table S1. Data table showing sample number, represented by distance from the EH in cm, δ^{238}U (in ‰) with associated uncertainty 2SD and number of runs (N), Th/U, U/Al, and %Dolomite in samples of this study

Sample (in cm from EH)	δ^{238}U (‰)	2SD	N	Th/U	U/Al	%Dolomite	δ^{13}C
1,000	−0.63	0.23	5	0.35	0.76	0.76	−0.17
880	−0.64	0.21	5	0.16	1.15	1.88	−0.83
802.5	−0.59	0.15	5	0.37	1.75	1.62	−0.21
727.5	−0.47	0.17	5	0.64	1.03	2.98	−0.26
672.5	−0.70	0.11	5	0.48	3.15	1.86	−1.07
610	−0.63	0.14	4	0.25	1.19	4.85	−0.29
585	−0.77	0.26	5	0.35	1.80	1.47	−0.09
522.5	−0.49	0.19	5	0.31	2.28	0.77	−0.20
500	−0.72	0.20	5	0.26	2.26	0.60	−1.23
435	−0.79	0.12	6	0.26	2.98	1.12	−0.34
421.5	−0.70	0.17	6	0.28	1.35	4.10	no data
395	−0.62	0.14	6	0.24	1.51	6.45	−0.28
362.5	−0.62	0.14	5	0.55	1.09	5.18	−0.05
310	−0.71	0.15	6	0.26	1.63	9.35	−0.10
292.5	−0.75	0.12	4	0.95	0.23	30.69	−0.04
131.5	−0.57	0.12	6	0.63	1.28	37.20	1.02
124.5	−0.58	0.12	6	0.65	0.34	21.87	0.30
92	−0.68	0.21	6	0.66	0.68	27.21	0.27
76	−0.66	0.17	6	0.36	1.25	18.57	0.66
51	−0.64	0.13	6	0.13	1.20	11.66	−0.37
33	−0.73	0.21	6	0.54	0.87	45.70	1.38
23	−0.64	0.13	3	0.40	0.95	51.14	0.88
15	−0.78	0.22	6	0.39	2.56	39.68	1.67
10.5	−0.48	0.17	7	0.51	0.88	32.37	1.82
8.2	−0.77	0.13	7	0.35	0.34	22.52	0.73
2.5	−0.46	0.09	4	0.58	0.53	36.45	0.05
−4	−0.64	0.08	8	0.16	5.30	0.69	0.56
−40	0.15	0.06	6	0.04	19.52	0.63	1.72
−64.5	−0.24	0.12	6	0.03	14.58	0.51	0.52
−97.5	−0.58	0.03	6	0.04	16.67	0.38	1.92
−117.5	−0.76	0.25	6	0.04	4.84	0.27	1.82
−160	−0.36	0.19	6	0.13	12.87	1.20	2.36
−270	−0.48	0.17	4	0.06	0.96	2.56	2.80
−330	−0.04	0.13	7	0.02	3.84	2.03	1.15
−370	−0.45	0.18	7	0.03	9.92	1.32	1.28
−389.5	−0.39	0.19	4	0.03	38.75	2.25	2.57
−409.5	−0.30	0.11	7	0.10	2.23	0.57	2.95

The δ^{13}C values are from (11) and are included here for reference. "N", the number of runs, refers to the times the sample was run for U isotopes. Multiple samples were run as replicates for quality control from powder, and these replicates are included in "N" as the same sample.